Highly selective immobilized bimetallic Ni-Au nanoparticle catalyst for the partial hydrogenation of m-dinitrobenzene

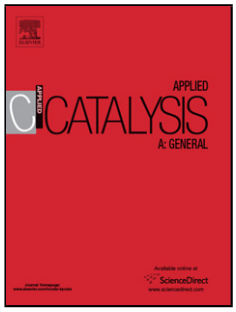

Title: Highly selective immobilized bimetallic Ni-Au nanoparticle catalyst for the partial hydrogenation of *m*-dinitrobenzene

Author: Daniel Lamey Oliver Beswick Fernando Cárdenas-Lizana Paul J. Dyson Esther Sulman Lioubov Kiwi-Minsker

PII: S0926-860X(17)30213-2
DOI: http://dx.doi.org/doi:10.1016/j.apcata.2017.05.015
Reference: APCATA 16237

To appear in: *Applied Catalysis A: General*

Received date: 4-4-2017
Revised date: 15-5-2017
Accepted date: 17-5-2017

Please cite this article as: D. Lamey, O. Beswick, F. Cárdenas-Lizana, P.J. Dyson, E. Sulman, L. Kiwi-Minsker, Highly selective immobilized bimetallic Ni-Au nanoparticle catalyst for the partial hydrogenation of *m*-dinitrobenzene., *Applied Catalysis A, General* (2017), http://dx.doi.org/10.1016/j.apcata.2017.05.015

Highly selective immobilized bimetallic Ni-Au nanoparticle catalyst for the partial hydrogenation of *m*-dinitrobenzene.

Daniel Lamey[1], Oliver Beswick[1], Fernando Cárdenas-Lizana[2], Paul J. Dyson[1], Esther Sulman[3] and Lioubov Kiwi-Minsker[1,3*]

[1] Institute of Chemical Sciences and Engineering, Ecole Polytechnique Fédérale de Lausanne (EPFL), CH-1015 Lausanne, Switzerland.

[2] Chemical Engineering, School of Engineering and Physical Sciences, Heriot-Watt University, Edinburgh EH14 4AS, Scotland.

[3] Regional Technological Centre, Tver State University, Zhelyabova Str., 33, Tver 170100, Russian Federation.

*Corresponding author: Lioubov Kiwi-Minsker: e-mail: Lioubov.kiwi-minsker@epfl.ch

Keywords: heterogeneous catalysis; nanoparticles; bimetallic nanoparticles; activated carbon fibres; structured catalysts; *m*-dinitrobenzene hydrogenation.

Abstract

Transition metal nanoparticles (NPs) are extensively used as catalysts for a wide and diverse range of organic transformations when immobilized on appropriate solid supports. We describe the development of a highly active and highly selective heterogeneous catalyst based on Ni-Au NPs supported on activated carbon fibers (ACFs) for the partial reduction of *m*-dinitrobenzene (*m*-DNB) to *m*-nitroaniline (*m*-NAN), an important platform chemical used in the synthesis of dyes and polymers. Initially, Ni NPs with narrow size distribution and ranging from 2 to 14 nm were prepared with poly-N-vinyl-2-pyrrolidone (PVP) as a stabilizer. Evaluation of the NPs as catalysts in the liquid-phase hydrogenation of *m*-dinitrobenzene led to the establishment of an antipathetic structure sensitivity, *i.e.* the larger NPs displayed a 6-fold higher turnover frequency than the smaller NPs. The selectivity to the target *m*-NAN product is independent of the size of the Ni NPs, possibly due to preferential PVP absorption of the NP edges and vertices. Consequently, Ni NPs of 2 nm were supported on ACFs and residual PVP was removed by a ultra-violet ozone (UVO) treatment, rendering a highly selective structured catalyst that affords *m*-NAN in almost 96% yield. A two-site (plane vs. edge Ni-atoms) Langmuir-Hinshelwood kinetic model is consistent with the experimental kinetic data confirming low-coordination atoms (edges and vertices) are responsible for selective reaction. Consequently, we prepared bimetallic Ni-Au NPs (Ni:Au = 1:1) aiming to

generate Ni surface sites mimicking the properties of edge and vertex atoms. The resulting UVO-treated Ni-Au NPs of 3 nm immobilized on ACFs afford *m*-NAN with a yield exceeding 98%. Such a high yield appears to be unprecedented and shows how careful nanocatalyst design, guided by detailed structural characterization and mechanistic studied, can lead to highly selective catalysts of industrial relevance.

1 Introduction

The majority of fine chemicals are manufactured using catalytic processes that diminish or even completely avoid the formation of unwanted by-products typical of non-catalytic processes. Most industrial processes still employ catalysts based on rare and expensive noble metals such as Rh and Pt[1] and, therefore, the development of new catalysts based on earth abundant transition metals such as Fe, Co, Ni, or mixtures of noble metals with earth abundant metals, is currently attracting considerable attention.[2] Active nanoparticle (NP) catalysts supported on high-surface-area solids[3] are of particular interest as the surface structure and the electronic properties of the NPs vary considerably in the low (< 3) nanometer range,[4] which strongly influences the reactions that take place on the NP surface. Differences in reactivity may be connected to the relative amount of plane, edge and vertex surface atoms which vary with NP size[5] and the size-sensitivity of catalytic reactions has been rationalized on the basis of structural and electronic factors.[6, 7] The electronic and

geometric properties of NPs may also be manipulated by the addition of a second metal, i.e. to generate bimetallic NPs,[8-11] which often show higher selectivity and reactivity than their monometallic counterparts. Indeed, during the last few years there has been a tremendous growth in interest in the application of bimetallic NPs in catalysis and, in particular, the use of Fe, Ni or Co in combination with noble metals.[12, 13]

NP catalysts have been extensively studied for the production of aromatic amines from aromatic nitro compounds, which are important intermediates in the manufacture of fine chemicals and end products,[14] and where selectivity is often a key issue.[15, 16] Notably, the partial hydrogenation of *m*-dinitrobenzene (*m*-DNB) to *m*-nitroaniline (*m*-NAN), *i.e.* via the selective reduction of one of the $-NO_2$ groups, is an important reaction as *m*-NAN is extensively used in the preparation of dyes and polymers.[17] Various factors influence the selectivity of this reaction including the type of metal,[18] the nanoparticle size,[19, 20] and even the nature of the support material.[21, 22] In addition to the catalyst, other parameters such as the polarity of the solvent,[23] or the use of modifiers[24] further influences the selectivity of the reaction.

NPs based on various transition metals, i.e. Pd,[25] Pt,[26] Ru[27] or Ni,[28, 29] catalyse the partial hydrogenation of *m*-DNB in the liquid phase. Compared to the noble metals, Ni is abundant and inexpensive and Ni NPs display remarkable efficiency in a number of catalytic reductions of nitroaromatic compounds, *e.g.* nitrobenzene,[30, 31] *p*-nitrophenol,[32] nitrotoluene, nitronaphtalene and dinitroaniline.[33] It has previously been shown that Ni NPs

(~2 nm diameter) impregnated on activated carbon fibres (ACF) are highly active catalysts for the hydrogenation of nitroarenes.[34] However, the influence on the size of the Ni NPs has not been explored in the liquid phase and bimetallic Ni-containing NPs have not been investigated. Consequently, more efficient catalysts for the partial hydrogenation of *m*-DNB may have been overlooked. Here, we describe a systematic investigation on Ni-based NPs catalysts for the selective hydrogenation of *m*-DNB to *m*-NAN, and the subsequent rational development of a highly active bimetallic Ni-Au NPs system immobilized on ACFs that afford *m*-NAN with an unprecedented selectivity of 98%.

2 Experimental

2.1 Materials

Nickel (II) sulfate hexahydrate (Fluka, ≥98.0%), Sodium tetrachloroaurate(III) dehydrate (Sigma-Aldrich, 99.9%), polyvinylpyrrolidone (PVP, Mw = 10'000/29'000, Sigma-Aldrich), ethylene glycol (Sigma-Aldrich, 99.8%), sodium hydroxide (Sigma-Aldrich, ≥98.0%), sodium borohydride (Sigma-Aldrich, ≥96.0%), tetraethylene glycol (Sigma-Aldrich, 99.0%), hydrogen peroxide (Reactolab SA, 30%), *m*-DNB (Tokyo Chemical Industry, ≥99.0%), methanol (MeOH, Sigma-Aldrich, ≥99.8%), ethanol (EtOH, Sigma-Aldrich, 99.8%), 1-propanol (Acros Organics, 95.5%), 1-butanol (Acros Organics, 95.5%) and 2-hexanol (Sigma-Aldrich, 99%) were used as received. Activated carbon fibers (ACFs, Kynol Europa GmbH, ~2'000 m^2 g^{-1}, produced from novoloid phenolic precursor fibers by a one step process combining carbonization and chemical activation) were employed for supporting the Ni and Ni-Au NPs (cf. below). All gases (H_2, N_2, and Ar) were of high purity (Carbagas, >99.7%).

2.2 Catalyst preparation

2.2.1 Unsupported Ni, Au and Ni-Au NPs

2 nm Ni NPs (Ni2): $NiSO_4 \cdot 6H_2O$ (0.053 g, 0.20 mmol) was dissolved in ethylene glycol (100 cm^3) and PVP (0.22 g, Mw = 10'000) was added. The mixture was stirred for 15 min and cooled to 273 K. NaOH (1 M in MiliQ, 5 cm^3) was added and the resulting solution was stirred for 90 min at 413 K. Acetone (1000 cm^3, 10:1 relative to the ethylene glycol) was used to precipitate the NPs (max. 240 min). After precipitation of the NPs, the supernatant was decanted and the remaining suspension was centrifuged. Following removal of the solvent layer the precipitate was re-dispersed in EtOH (15 cm^3).

4 nm Ni NPs (Ni4): $NiSO_4 \cdot 6H_2O$ (0.26 g, 0.99 mmol) was dissolved in ethylene glycol (50 cm^3) and PVP (2.2 g, Mw = 29'000) was added. Freshly dissolved $NaBH_4$ in water (0.53 M in MiliQ, 5 cm^3) was added, leading to instantaneous particle nucleation (indicated by a change of color to black/brown). Then, the solution was stirred for 240 min at 293 K. Acetone (500 cm^3, 10:1 relative to the ethylene glycol) was used to precipitate the NPs (max. 240 min). After precipitation of the NPs, the supernatant was decanted and the remaining suspension was centrifuged. Following removal of the solvent layer the precipitate was re-dispersed in EtOH (15 cm^3).

11 nm Ni NPs (Ni11): $NiSO_4 \cdot 6H_2O$ (0.26 g, 0.99 mmol) was dissolved in ethylene glycol (120 cm^3). PVP (2.2 g, Mw = 29'000), NaOH (1 M in MiliQ, 4 cm^3) and hydrazine hydrate

(1 M in MiliQ, 2 cm^3) were added. The solution was then brought to reflux for 240 min. Acetone (1000 cm^3, 10:1 relative to the ethylene glycol) was used to precipitate the NPs (max. 240 min). After precipitation of the NPs, the supernatant was decanted and the remaining suspension was centrifuged. Following removal of the solvent layer the precipitate was re-dispersed in EtOH (15 cm^3).

14 nm Ni NPs (Ni14): $NiSO_4 \cdot 6H_2O$ (0.26 g, 0.99 mmol) was dissolved in tetra-ethyleneglycol (120 cm^3). PVP (2.2 g, Mw = 29'000) and NaOH (1 M, 5 cm^3) were added to that solution which was finally brought to reflux for 240 min. Acetone (1000 cm^3, 10:1 relative to the tetra-ethylene glycol) was used to precipitate the NPs (max. 240 min). After precipitation of the NPs, the supernatant was decanted and the remaining suspension was centrifuged. Following removal of the solvent layer the precipitate was re-dispersed in EtOH (15 cm^3).

7 nm Au NPs (Au7): $NaAuCl_4 \cdot 2H_2O$ (0.010 g, 0.025 mmol) was dissolved in water (MiliQ, 5 cm^3) and combined with PVP (0.010 g, 0.0875 mmol) dissolved in ethylene glycol (90 cm^3). The mixture was stirred for 120 min at 353 K and cooled down to 273 K. and the pH was adjusted to *ca*. 9 by adding NaOH (1 M in MiliQ water, 5 cm^3). The mixture was then stirred for 90 min at 373 K yielding in a crude NP dispersion. Acetone (1000 cm^3, 10:1 relative to the ethylene glycol) was used to precipitate the NPs (max. 240 min). The supernatant was decanted and the remaining suspension was centrifuged. Following removal of the solvent layer the precipitate was re-dispersed in EtOH (15 cm^3).

3 nm Ni@Au NPs (Ni-Au): $NaAuCl_4 \cdot 2H_2O$ (0.08 g, 0.20 mmol), $NiSO_4.6H_2O$ (0.05 g, 0.20 mmol) and PVP (Mw = 10000, 0.222 g,) were dissolved in ethanol (150 cm^3). The mixture was stirred for 60 min at 293 K. Freshly dissolved $NaBH_4$ in EtOH (0.12 M, 10 cm^3) was added, leading to the instantaneous particle nucleation (indicated by a change of color to black/brown). The solution was stirred for a further 2 h. Acetone (500 cm^3, 10:1 relative to the ethylene glycol) was used to precipitate (max. 240 min) the NPs. Following precipitation of the NPs, the supernatant was decanted and the remaining suspension was centrifuged. Following removal of the solvent layer the precipitate was collected and washed twice with hexane:EtOH (1:1, 10 cm^3) then water (MiliQ, 3 x 10 cm^3) and finally re-dispersed in EtOH (15 cm^3).

2.2.2 Supported catalysts

Supported catalysts were prepared by deposition (impregnation) of the Ni and Ni-Au NPs on a structured support of activated carbon fibers (ACFs). Prior to deposition, the ACFs were activated in 15% nitric acid (20 min, 363 K) to create high concentration of oxygen-containing groups on the carbon surface.[35] Treated ACFs were impregnated with an ethanolic suspension containing the appropriate NPs (0.03 g of ACFs were impregnated by 0.7 cm^3 of 0.01 M Ni, Au or Ni-Au NPs solutions) and then dried for 2 h. Next, the Ni/ACF and Ni-Au/ACF were subjected to either a UV-ozone (UVO) or thermal treatment to remove the PVP stabilizer.[36, 37] For PVP removal by UVO the catalyst was placed for 4 h under an

UV lamp in air (λ = 185 nm and 257 nm, which generates ozone) . PVP removal by thermal treatment involved pyrolysis in a flow of 100 $cm^3 \cdot min^{-1}$ 20% v/v H_2/Ar at 2 $K \cdot min^{-1}$ to 873 K (2 h). Samples were passivated at room temperature in 1% v/v O_2/Ar a to prevent a strong bulk oxidation of Ni. The metal content of supported NP catalysts was quantified by AAS (see below).

2.3 Catalyst Characterization

High resolution scanning electron microscopy (HRSEM) was performed using a Philips FEI XL30-FEG equipped with an Everhart-Thornley secondary-electron (SE) detector using an accelerating voltage between 10□13 kV, or with a Carl Zeiss MERLIN FE-SEM equipped with two annular and Everhart-Thornley secondary-electron (SE) detectors operated at an accelerating voltage of 5□30 keV with a beam current of 1.0□3.0 nA and using ZeissSmartSEM software for data acquisition/manipulation.

High resolution transmission electron microscopy (HRTEM) was performed using a JEOL JEM-3011 instrument. The electron optical parameters were set as follows: Cs = 0.6 mm, Cc = 1.2 mm, electron energy spread = 1.5 eV and beam divergence semi-angle = 1 mrad. Gatan Digital Micrograph was used for data treatment. Specimens for analysis were prepared from dispersions in EtOH by deposition on a holey carbon/Cu grid (Agar Scientific, 300 Mesh). Up to 250 individual NPs were counted for each sample and the mean diameter (*d*) was calculated using:

$$d = \frac{\sum_i n_i d_i}{\sum_i n_i} \quad (1)$$

where n_i is the number of particles of diameter d_i.

Energy Dispersive X-Ray (EDX) analysis was performed using a 7 nm beam diameter, PGT prism Si/Li detector and an Avalon 2000 analytical system.

X-Ray Diffraction (XRD) were collected on a Roentgen PW3040/60 XPert PRO powder Xray diffractometer with a high resolution PW3373/00 Cu LFF (unmonochromated) tube at λ = 1.5404 Å (Cu Kα). Samples were prepared by solvent evaporation from NP suspensions deposited on the 0.5 mm deep ground area of a glass flat-plate sample holder using a microscope slide to ensure a smooth, flat and flush sample with respect to the sample holder surface. The holder was inserted onto the sample stage (PW3071/60 Bracket) such that the sample was just free of the reference plane of the sample stage.

Atomic absorption spectroscopy (AAS) was carried out using a Shimadzu AA-6650 spectrometer to determine the metal content of the supported catalysts. Samples were calcined in air at 873 K for 2 h and the remaining solid (metal oxide) was dissolved in aqua regia (HNO_3:HCl (v/v) = 1:3) and diluted in demineralized water.

2.4 Hydrogenation of *m*-DNB

Hydrogenation reactions (T = 423 K; P_{H_2} = 6□20 bar) were carried out in a batch stirred reactor (100 cm^3 stainless steel autoclave, Büchi AG, Switzerland) equipped with a pressure controlled H_2 supply system. A methanolic solution of *m*-DNB ($C_{m\text{-DNB}} = 3.7 \times 10^{-3}$ mol·l^{-1}, 80 cm^3) was added to the autoclave and the system was flushed three times with N_2 under agitation. The NPs were introduced by injection into the reactor as ethanolic solutions (0.08□0.38 cm^3) to reach the desired *m*-DNB to Ni molar ratio. The supported catalysts were fixed mechanically between wire-mesh blades (4) attached directly to the stirrer shaft and removable ones. The mass of structured catalyst (15□30 mg) was adjusted to reach the desired *m*-DNB to Ni molar ratio. A re-circulator (HAAKE B-N3) was used to stabilize the reaction temperature to within ± 1 K (*ca.* 1 h) using mineral oil (Shell Thermia; thermal conductivity = 0.45 kJ·m^{-1}·h^{-1}·K^{-1}; specific heat = 2.4 kJ·kg^{-1}·K^{-1}) as the thermal medium. Hydrogen was then introduced and the system was pressurized to 20 ± 0.2 bar (up to 11-fold excess of the stoichiometric requirements for hydrogenation to *m*-NAN) and stirring was started (reaction time, t = 0). No measurable conversion was detected in the absence of a catalyst. The initial –NO_2/Ni molar ratio spanned the range 28□58. A liquid sampling system composed of a 1/8 inch stainless steel tube surrounded by two quarter turn plug valves allowed aliquots (≤ 0.4 cm^3) of the reaction mixture to be removed when required.

Sample composition was analyzed using a Perkin-Elmer Clarus 500 chromatograph equipped with a programmed split/splitless injector and a flame ionization detector employing a Stabilwax

(Cross-bond Carbowax-PEG, Restek, USA) capillary column (i.d. = 0.32 mm, length = 30 m, film thickness = 0.25 μm). Data acquisition/manipulation were performed using the TotalChrom Workstation v.6.3.2. chromatography data system and the concentration of organic species in the bulk liquid (C_i) phase were determined from the total mass balance in the reaction mixture. The conversion of *m*-DNB ($X_{m\text{-DNB}}$) is defined as:

$$X_{m\text{-DNB}}(\%) = \frac{C_{m\text{-DNB},0} - C_{m\text{-DNB,i}}}{C_{m\text{-DNB},0}} \times 100 \quad (2)$$

and selectivity with respect to *m*-nitroaniline ($S_{m\text{-NAN}}$) as a target product is given as:

$$S_{m-\text{NAN}}(\%) = \frac{C_{m-\text{NAN}}}{C_{m-\text{DNB},0} - C_{m-\text{DNB}}} \times 100 \quad (3)$$

The *m*-NAN yield with respect to *m*-DNB is defined as:

$$Y_{m-\text{NAN}}(\%) = \frac{C_{m-\text{NAN,i}}}{C_{m-\text{DNB},0}} \cdot \frac{\nu_{m-\text{DNB}}}{\nu_{m-\text{NAN}}} \times 100 \quad (4)$$

Repeated reaction runs with the same batch of catalyst delivered yields that were reproducible within ± 0.5%. No leaching of Ni in the solution after the reaction has been detedted by Atomic Absorption spectroscopy. The only detected product other than *m*-NAN was *m*-phenylenediamine (*m*-PDA).

The catalytic activity was quantified in terms of the initial *m*-DNB consumption rate ($-R_{m\text{-DNB},0}$) determined from a linear regression of the temporal *m*-DNB concentration profile:

$$-R_{m\text{-DNB},0}\ (\text{mol}_{m\text{-DNB}}\text{mol}_{\text{Ni}}^{-1}\ \text{min}^{-1}) = \frac{(C_{m-\text{DNB},0} - C_{m\text{-DNB}}) \cdot V}{n_{\text{Ni}} \cdot t_{\text{R}}} \quad (5)$$

where V is the reaction volume, n_{Ni} is the number of moles of Ni, and t_R the reaction time.

Alternatively, the turnover frequency (TOF):

$$TOF\ (\mathrm{min}^{-1}) = \frac{-R_{m\text{-DNB},0}}{D} \quad (6)$$

where D is the average NP dispersion, defined by the ratio of surface atoms to the total number of atoms.

3 Results and discussion

3.1 Preparation and characterization of the Ni NPs

The size of NPs depends on the proportion of particle nucleation relative to particle growth during their formation,[38] which in practical terms is influenced by several synthesis parameters like a reducing agent strength, temperature, solvent, pH and type of stabilizer to prevent agglomeration. Typically, other things being equal, strong reducing agents ($NaBH_4$) favor the formation of smaller NPs as these reducing agents induce rapid nucleation, whereas weak reducing agents, *e.g.* polyols, result in the formation of larger NPs due to reduced nucleation and NP growth mechanisms dominating. Consequently, we prepared a series of Ni NPs of different sizes (see below) from $NiSO_4 \cdot 6H_2O$ employing PVP as a stabilizer with a

series of different reducing agents. Details are given in the Experimental and reaction conditions are summarized in Table 1.

Table 1

The Ni NPs were characterized by TEM and HRSEM (Figs. 1, S1 and S2), revealing spherical morphologies with cubo-octahedral shape.[39] From the associated size distribution graphs (Figs. 1B, S1B and S2B) the average size of the Ni NPs was determined as 2 nm (prepared using ethylene glycol, termed Ni2), 4 nm (prepared using $NaBH_4$, termed Ni4), 11 nm (prepared using hydrazine hydrate, termed Ni11) and 14 nm (prepared using tetra-ethyleneglycol, termed Ni14). Moreover, the histograms showed narrow size distributions of the NPs.

Figure 1

3.2 Evaluation of the Ni NPs in the catalytic partial hydrogenation of *m*-DNB

The Ni NPs (Ni2, Ni4, Ni11 and Ni14 nm) were evaluated as catalysts in the liquid-phase hydrogenation of *m*-DNB in MeOH (see Figure 2). MeOH was selected following a screening of multiple solvents with the selectivity towards *m*-NAN being the primary criterion (cf. Fig.

S3). Interestingly, the turnover frequency (TOF) of the Ni14 NPs is 6-fold higher than that observed for the Ni2 NPs, which is consistent with an antipathetic structure sensitivity.[40] To the best of our knowledge, size effects of Ni NPs in liquid phase hydrogenation of *m*-DNB have not been reported.

Figure 2

NP size influences the TOF of a reaction due to electronic and geometric effects[41] and the relative ratio of the different types of surface atoms (edge, vertex and plane atoms), which changes substantially with particle size, i.e. larger NPs possess mainly large crystal planes with atoms of high coordination number, whereas in smaller NPs metal atoms with low coordination numbers are more prevalent. The non-ideal face-centered cubo-octahedron (fcc) model established by Hardeveld et al.[42] was used to determine the relative number of different atom types present on the surfaces of the different Ni NPs and the corresponding surface atoms fractions (x_i) are reported in Table 2. Ni atoms with low coordination numbers, *i.e.* edge and vertex atoms, dominate in the Ni2 NPs whereas planes dominate the Ni14 NPs suggesting that plane Ni atoms are more active for the hydrogenation of *m*-DNB. The correlation between the TOF and planes fraction ($\boldsymbol{x_{\sigma 1}}$) with the NPs size is shown in Figure 2. This is probably linked to a stronger interaction of the $-NO_2$ group in the *m*-DNB substrate on the plane atoms.[43]

Table 2

The selectivity to the partially hydrogenated *m*-NAN product, always balanced by the *m*-PDA selectivity, was found to be essentially independent of the NP size, corresponding to 78±3% at a conversion of 50% and decreasing to 35±3% at a conversion of 99% (Figure 2B). This effect could be due to the influence of the PVP used as a stabilizing agent, despite removing excess PVP via extensive washing and re-dispersion of the NPs in EtOH (see Experimental for details).[44] PVP adsorbs preferentially on the edges and vertices of NPs (i.e. low coordination number sites compared to plane atoms). The existence of different strengths of adsorption between structure-directing agent and surface atoms with distinct miller indices have been demonstrated by density functional theory (DFT) calculations.[45, 46] Consequently, the low selectivity to the target product which is independent of the size of the Ni particle suggests that edge and vertex atoms are probably responsible for the reaction selectivity, but in the disperse NPs they are blocked by PVP.

3.3 Preparation and characterization of Ni NPs supported on ACFs

Ni2 and Ni14 NPs were supported on ACFs and treated by UV-Ozone (UVO) or pyrolysis (ΔT) under an inert gas in order to remove residual PVP from the nickel surfaces (see Experimental for details). These catalysts are referred as Ni/ACF_{UVO} or Ni/$ACF_{\Delta T}$, respectively. Representative HRSEM images of the Ni NPs after PVP removal by UVO treatment or pyrolysis are shown in Figure S2. Only slight particle growth is observed following UVO treatment (Ni2: $2.0 \rightarrow 2.3$ nm; Ni14: no change) whereas extensive Ni

sintering occurs during the thermal treatment process (Ni2: 2.0 → 26 nm; Ni14: 14.0 → 30 nm).

PVP traces are believed to have a detrimental effect on the selectivity of the reaction due to their preferential adsorption on edges and vertices (see above). Using the PVP-free supported Ni/ACF catalysts a remarkable increase in selectivity to *m*-NAN (from 35% up to 96%) at 99% *m*-DNB conversion was observed (Figure 3). Moreover, the smaller (2 nm) supported NPs were found to provide the highest selectivity, confirming that the low coordination Ni atoms (in the edges and vertices) are responsible for the high selectivity, since the smaller NPs have a high ratio of these atoms relative to planes, and that these sites appear to be fully accessible when the PVP is removed from the surface of the NPs.

Figure 3

The substrate and product distribution as a function of time for the Ni2/ACF_{UVO} catalyst is shown in Figure 4A. The *m*-DNB substrate is converted quasi-exclusively to *m*-NAN with a zero order kinetics (linear dependence of the concentration *vs.* time), up to 75% *m*-DNB conversion, with only a small amount ($\leq 5\%$) of the fully hydrogenated product, *m*-phenylenediamine (*m*-PDA). Comparison of the selectivity to *m*-NAN as a function of conversion for the unsupported PVP-stabilized Ni NPs *vs.* Ni/ACF_{UVO} catalysts (Figures 4B, 4C) reveals that the highest selectivity to *m*-NAN was recorded over the supported NPs. The Ni2/ACF_{UVO} catalyst is the most selective ($S_{m\text{-NAN}} \geq 95\%$ up to X = 98%). In contrast, there is

a continuous decrease in selectivity for unsupported Ni2 and Ni14 NPs as the conversion increases. Consecutive/parallel reaction pathways are depicted in Figure 5 presenting a simplified reaction scheme.

Figure 4

Figure 5

3.4 Kinetic modelling

The observed catalytic behavior of the Ni2 and Ni14 and Ni2/ACF_{UVO} and Ni14/ACF_{UVO} systems was modelled by applying a Langmuir-Hinshelwood mechanism assuming two types of active sites, dissociative hydrogen adsorption and bimolecular reactions between the adsorbed species. The detailed derivation of the reaction rate expressions is based on the scheme presented in Figure 5 (see supplementary content for further details). The rate equations were developed as follows, using subscripts D, N and P refer to *m*-DNB, *m*-NAN and *m*-PDA, respectively while DH, DH2, DH3 and NH correspond to the reaction intermediates:

$$r_1 = \frac{k'_{1,\sigma_1} K_{D,\sigma_1} C_D}{\left(1 + K_{D,\sigma_1} C_D + K_{N,\sigma_1} C_N\right)^2} \tag{7}$$

$$r_3 = \frac{k'_{3,\sigma_2} K_{D,\sigma_2} C_D}{\left(1 + K_{D,\sigma_2} C_D + K_{N,\sigma_2} C_N\right)^2} \tag{8}$$

$$r_2 = \frac{k'_{2,\sigma_1} K_{N,\sigma_1} C_N}{\left(1 + K_{D,\sigma_1} C_D + K_{N,\sigma_1} C_N\right)^2} \quad (9)$$

$$r_4 = \frac{k'_{4,\sigma_1} K_{D,\sigma_1} C_D}{\left(1 + K_{D,\sigma_1} C_D + K_{N,\sigma_1} C_N\right)^2} \quad (10)$$

The mass balance for *m*-DNB, *m*-NAN and *m*-PDA are given by:

$$\frac{dC_D}{dt} = -r_1 - r_3 - r_4 \quad (11)$$

$$\frac{dC_N}{dt} = r_1 + r_3 - r_2 \quad (12)$$

$$\frac{dC_P}{dt} = r_2 + r_4 \quad (13)$$

The parallel *m*-DNB $\rightarrow$ *m*-PDA path was taken into consideration for the Ni14 NPs, as a small amount of over-hydrogenation is observed at low conversions (< 5%). Therefore, equation (8) (of supplementary content) and the contribution of r_4 in the mass balance were considered for the larger NPs. Equations (7-10) were solved (using Berkeley Madonna software v.8.3.18 with Runge-Kutta's method for differential equations). A good correlation between the model and experimental values was obtained for the four systems (see Figure 6). It is worth noting that all catalysts required a short ($\leq$ 10% of the total reaction time) induction period, presumably due to activation of the catalyst in the reaction mixtures[47] or to surface restructuring processes.[48] The former is considered more likely in the presence of H_2 which re-reduces any passivated surface layer.[34] The induction periods were not included in the kinetic curves simulations.

Figure 6

The adsorption and kinetic constants obtained are listed in Table 3. Similar values were fixed for the individual adsorption constants, which are slightly higher (< 2-fold) for the Ni2/ACF_{UVO} catalyst compared to the solvent dispersed Ni2 catalyst. The interaction of the *m*-DNB substrate is stronger (by about two orders of magnitude) with plane atoms (σ_1 sites) compared to the adsorption on edge and vertex atoms (σ_2 sites). The origin for this difference could come from the mode of adsorption with vertical (involving only one NO_2-group) on the edges and parallel to the crystallographic face on the plane atoms. By the same logic, the partially reduced *m*-NAN exhibit 10-fold higher adsorption constant ($K_{N,\sigma1}$**)** in comparison with *m*-DNB ($K_{D,\sigma2}$). For the Ni/ACF_{UVO} catalysts the kinetic constant, k_3, related to the *m*-DNB to *m*-NAN hydrogenation steps on σ_2 sites is significantly higher (5- to 10-fold) than k_3 for the dispersed Ni NPs. Thus, with the dispersed Ni NPs the first hydrogenation step takes place predominantly on σ_1 sites since the σ_2 sites are largely blocked by PVP. High k_3/k_1 and k_3/k_2 ratios demonstrates the key role of σ_2 sites in the first hydrogenation step with minimized over-hydrogenation, and accounts for the high selectivity of the Ni2/ACF_{UVO} catalyst.

Table 3

3.5 Development of a bimetallic Ni-Au/ACF catalyst

The catalytic performance of the Ni NPs (see above) implies the key role of low coordination number Ni atoms to achieve high selectivity to *m*-NAN. Consequently, an active

phase consisting of single Ni atoms could be highly effective and, therefore, Ni-Au NPs were prepared together with Au NPs for comparison purposes. The Au NPs were prepared in the same way as that described for the Ni NPs, i.e. from $NaAuCl_4$ in the presence of PVP using NaOH as the reductant. The corresponding HRTEM images (Figure 7A, C) reveal spherical Au NPs, albeit with some degree of agglomeration, with a mean diameter of 6.9 ± 1.5 nm (Au7).

Figure 7

The Ni-Au NPs were synthesized by reduction of $NiSO_4$ and $NaAuCl_4$ (1:1) with $NaBH_4$ employing PVP as a stabilizer and the HRTEM images and associated size distribution graph of the bimetallic NPs are shown in Figure 7. The Ni-Au NPs have an average size of 2.7 ± 0.7 nm and the EDX spectrum (Figure 8) confirms the presence of gold and nickel in a single NP. The bulk binary Ni-Au phase diagram[49] has a large miscibility gap excluding Ni-Au alloy formation at low temperatures. However, it has been shown by STM[9], low energy ion scattering and low energy electron diffraction[50] and Monte Carlo simulations in combination with *in situ* X-ray absorption fine structure studies[51] that a surface alloy between Au and Ni can exist in small NPs.

Figure 8

Figure 9 shows the XRD diffractograms in the range 30□50° for monometallic Ni and Au

NPs in comparison with the bimetallic Ni-Au NPs. The two main peaks for the Ni-Au NPs are observed at 38.3° (111) and 44.1° (200) indicating that the fcc crystallographic structure corresponds to the one of the monometallic gold (Au7) with a cell parameter of 4.09 ± 0.02 Å. The Ni-Au NPs prepared in this work differ from those previously reported which exhibit peaks as a combination of the metallic components (Ni and Au) and shrinkage of the lattice structure.[52, 53] It indicates the absence of bulk alloy in the prepared bimetallic NPs. The larger peak width for the Ni-Au NPs sample could be due to the higher dispersion (2.7 nm), which is in line with the HRTEM images.

Figure 9

The Ni-Au NPs were evaluated as a catalyst in the liquid-phase hydrogenation of *m*-DNB in comparison to the Ni2 and Au7 NPs (Figure 10). Notably, the catalytic activity of all the NPs is of the same order of magnitude, whereas they exhibit considerable differences in selectivity. At close to full conversion ($X_{m\text{-DNB}}$ = 99%), the Au NPs affords mostly the fully hydrogenated product, *m*-PDA (selectivity towards *m*-NAN < 5%). The Ni NPs are somewhat more selective with about 35% *m*-NAN obtained. Gold is more electronegative than Ni, indicating that a more electron rich surface is detrimental to the selectivity of the reaction towards the *m*-NAN product. In contrast, the Ni-Au NPs afforded almost exclusively the desired *m*-NAN product ($S_{m\text{-NAN}}$ = 99%). Such a high selectivity may be attributed to the high dispersity of Ni atoms in the bimetallic Ni-Au NPs and, due to the presence of the electronegative Au atoms, the increased electropositive character of the surface Ni atoms.

Figure 10

ACF supported Ni-Au NPs were prepared in the same way described for the Ni2/ACF_{UVO} system (see Experimental). The initial reaction rate was 3-fold higher for the Ni-Au/ACF_{UVO} catalyst and, importantly, the selectivity towards the desired product ($S_{m\text{-NAN}}$ = 99%) was preserved allowing *m*-NAN to be obtained in > 98% yield. In comparison, the yield of *m*-NAN obtained over the best monometallic supported Ni (Ni2/ACF_{UVO}) catalyst was slightly lower (96%). To the best of our knowledge, a yield of *m*-NAN exceeding 98% is unprecedented for a Ni-based catalysts, although a yield of 94% was previously achieved using Ni-Ag core-shell NPs but hydrazine was used instead of hydrogen as a reducing agent.[54] We believe that the use of structure fibrous (ACF) catalysts allowing to design flow reactors for hydrogenation [55] should bring supplemental advantages in technical applications.

Conclusions

Ni NPs with narrow size distribution and mean diameters between 2□14 nm were prepared using PVP as a stabilizing agent and evaluated as catalysts in the partial hydrogenation of *m*-DNB to *m*-NAN. The catalytic activity of the NPs expressed as TOF increased with the NP size, however, the selectivity of the reaction was low and over-hydrogenation to *m*-PDA was observed, especially at high conversions of *m*-DNB. Edge and vertex Ni atoms were shown to

afford the desired *m*-NAN product whereas plane atoms preferentially lead to fully hydrogenated *m*-PDA. The low selectivity of the Ni NPs was attributed to preferential adsorption of the PVP stabilizer on the edge and vertex Ni atoms, consistent with a two-site Langmuir-Hinshelwood kinetic model developed to rationalize the obtained results. Immobilization of the smallest Ni NPs (2 nm) on ACFs followed by removal of the PVP from the NP surfaces via UVO treatment afforded a Ni2/ACF_{UVO} catalyst that was considerably more selective to the partial hydrogenation product at close to full substrate conversion, i.e. the yield of *m*-NAN approaches 96%.

Based on the selectivity mechanism, i.e. that low Ni coordination sites lead to the high selectivity, bimetallic Ni-Au NP (Ni:Au = 1:1) PVP-stabilized were prepared aiming to mimic the properties of surface atoms with low coordination number (*e.g.* edges and vertices). Indeed, the selectivity of the dispersed Ni-Au towards *m*-NAN compared to the monometallic Ni and Au NPs was significantly higher. This synergy was additionally ascribed to the more electropositive character of the Ni atoms due to the electron-withdrawing effect of the electronegative Au atoms. Finally, immobilization of the Ni-Au NPs on ACFs followed by UVO treatment gives a supported heterogeneous catalyst that affords *m*-NAN in > 98% yield. Such a high selectivity appears to be unprecedented and shows how careful nanocatalyst design, guided by detailed structural characterization and mechanistic studied, can lead to highly selective catalysts of industrial relevance.

Acknowledgment

We thank Dr. Pavel Abdulkin for help preparing the Ni NPs and Sara Moya-Pascual for help with the catalytic studies. We thank the Swiss National Science Foundation and the Russian Science Foundation (project 15-19-20023) for financial support.

Conflict of interest statement

We certify that there is no conflict of interest with any financial organization regarding the material discussed in this manuscript.

4 References

[1] U.K. Singh, M.A. Vannice, Kinetics of liquid-phase hydrogenation reactions over supported metal catalysts - a review, Appl Catal a-Gen, 213 (2001) 1-24.
[2] J. Pal, T. Pal, Faceted metal and metal oxide nanoparticles: design, fabrication and catalysis, Nanoscale, 7 (2015) 14159-14190.
[3] C.-J. Jia, F. Schuth, Colloidal metal nanoparticles as a component of designed catalyst, Physical Chemistry Chemical Physics, 13 (2011) 2457-2487.
[4] P. Claus, A. Bruckner, C. Mohr, H. Hofmeister, Supported gold nanoparticles from quantum dot to mesoscopic size scale: Effect of electronic and structural properties on catalytic hydrogenation of conjugated functional groups, Journal of the American Chemical Society, 122 (2000) 11430-11439.
[5] M. Crespo-Quesada, A. Yarulin, M.S. Jin, Y.N. Xia, L. Kiwi-Minsker, Structure Sensitivity of Alkynol Hydrogenation on Shape- and Size-Controlled Palladium Nanocrystals: Which Sites Are Most Active and Selective?, Journal of the American Chemical Society, 133 (2011) 12787-12794.
[6] N. Semagina, L. Kiwi-Minsker, Recent Advances in the Liquid-Phase Synthesis of Metal Nanostructures with Controlled Shape and Size for Catalysis, Catal Rev, 51 (2009) 147-217.
[7] C.O. Bennett, M. Che, Some Geometric Aspects of Structure Sensitivity, J Catal, 120 (1989) 293-302.
[8] J.H. Sinfelt, Bimetallic catalysts : discoveries, concepts, and applications, Wiley, New York, 1983.
[9] L.P. Nielsen, F. Besenbacher, I. Stensgaard, E. Laegsgaard, C. Engdahl, P. Stoltze, K.W. Jacobsen, J.K. Norskov, Initial Growth of Au on Ni(110) - Surface Alloying of Immiscible Metals, Phys Rev Lett, 71 (1993) 754-757.
[10] F. Besenbacher, I. Chorkendorff, B.S. Clausen, B. Hammer, A.M. Molenbroek, J.K. Norskov, I. Stensgaard, Design of a surface alloy catalyst for steam reforming, Science, 279 (1998) 1913-1915.

[11] A.K. Singh, Q. Xu, Synergistic Catalysis over Bimetallic Alloy Nanoparticles, Chemcatchem, 5 (2013) 652-676.
[12] B. Narayanamoorthy, V. Linkov, C. Sita, S. Pasupathi, Pt3M (M: Co, Ni and Fe) Bimetallic Alloy Nanoclusters as Support-Free Electrocatalysts with Improved Activity and Durability for Dioxygen Reduction in PEM Fuel Cells, Electrocatalysis-Us, 7 (2016) 400-410.
[13] S. Diodati, E. Negro, K. Vezzu, V. Di Noto, S. Gross, Oxygen reduction reaction and X-ray photoelectron spectroscopy characterisation of carbon nitride-supported bimetallic electrocatalysts, Electrochim Acta, 215 (2016) 398-409.
[14] R.S. Downing, P.J. Kunkeler, H. vanBekkum, Catalytic syntheses of aromatic amines, Catal Today, 37 (1997) 121-136.
[15] G.J. Hutchings, Heterogeneous catalysts-discovery and design, Journal of Materials Chemistry, 19 (2009) 1222-1235.
[16] H.U. Blaser, C. Malan, B. Pugin, F. Spindler, H. Steiner, M. Studer, Selective hydrogenation for fine chemicals: Recent trends and new developments, Advanced Synthesis & Catalysis, 345 (2003) 103-151.
[17] V.L. Khilnani, S.B. Chandalia, Selective hydrogenation. II. m-dinitrobenzene to m-nitroaniline using palladium on carbon as catalyst, Org Process Res Dev, 5 (2001) 263-266.
[18] H.U. Blaser, H. Steiner, M. Studer, Selective Catalytic Hydrogenation of Functionalized Nitroarenes: An Update, Chemcatchem, 1 (2009) 210-221.
[19] K. Shimizu, Y. Miyamoto, A. Satsuma, Size- and support-dependent silver cluster catalysis for chemoselective hydrogenation of nitroaromatics, Journal of Catalysis, 270 (2010) 86-94.
[20] F. Cárdenas-Lizana, S. Gómez-Quero, H. Idriss, M.A. Keane, Gold Particle Size Effects in the Gas-Phase Hydrogenation of *m*-dinitrobenzene over Au/TiO_2, J Catal, 268 (2009) 223-234.
[21] S.A. Regenhardt, C.I. Meyer, T.F. Garetto, A.J. Marchi, Selective gas phase hydrogenation of maleic anhydride over Ni-supported catalysts: Effect of support on the catalytic performance, Appl Catal a-Gen, 449 (2012) 81-87.
[22] F. Cárdenas-Lizana, S. Gómez-Quero, M.A. Keane, Clean Production of Chloroanilines by Selective Gas Phase Hydrogenation Over Supported Ni Catalysts, Applied Catalysis A: General, 334 (2008) 199-206.
[23] R.A. Rajadhyaksha, S.L. Karwa, Solvent Effects in Catalytic-Hydrogenation, Chem Eng Sci, 41 (1986) 1765-1770.
[24] C. Exner, A. Pfaltz, M. Studer, H.U. Blaser, Heterogeneous enantioselective hydrogenation of activated ketones catalyzed by modified Pt-catalysts: A systematic structure-selectivity study, Advanced Synthesis & Catalysis, 345 (2003) 1253-1260.
[25] V.L. Khilnani, S.B. Chandalia, Selective hydrogenation. I. para-chloronitrobenzene to para-chloroaniline platinum on carbon as catalyst, Org Process Res Dev, 5 (2001) 257-262.
[26] H. Rojas, G. Borda, P. Reyes, M. Brijaldo, J. Valencia, Liquid-Phase Hydrogenation of M-Dinitrobenzene over Platinum Catalysts, J Chil Chem Soc, 56 (2011) 793-798.
[27] S.L. Zhao, H.D. Liang, Y.F. Zhou, Selective hydrogenation of m-dinitrobenzene to m-nitroaniline. catalyzed by PVP-Ru/Al2O3, Catalysis Communications, 8 (2007) 1305-1309.
[28] Y.X. Liu, Z.J. Wei, S.G. Deng, J.Y. Zhang, Hydrogenation of m-dinitrobenzene to m-phenylenediamine over La2O3-promoted Ni/SiO2 catalysts, J Chem Technol Biot, 84 (2009) 1381-1389.
[29] M.M. Telkar, J.M. Nadgeri, C.V. Rode, R.V. Chaudhari, Role of a Co-Metal in Bimetallic Ni–Pt Catalyst for Hydrogenation of m-Dinitrobenzene to m-Phenylenediamine, Appl Catal a-Gen, 295 (2005) 23-30.

[30] J.H. Wang, Z.L. Yuan, R.F. Nie, Z.Y. Hou, X.M. Zheng, Hydrogenation of Nitrobenzene to Aniline over Silica Gel Supported Nickel Catalysts, Ind Eng Chem Res, 49 (2010) 4664-4669.
[31] K.J.A. Raj, M.G. Prakash, R. Mahalakshmy, T. Elangovan, B. Viswanathan, Liquid Phase Hydrogenation of Nitrobenzene over Nickel Supported on Titania, Chinese J Catal, 33 (2012) 1299-1305.
[32] R. Chen, Y. Du, W. Xing, N. Xu, Effects of Alumina Particle Size and Nickel Loading on Ni/Al_2O_3 Catalysts for *p*-Nitrophenol Hydrogenation, J. Chem. Technol. Biotechnol., 15 (2008) 884-888.
[33] R.J. Kalbasi, A.A. Nourbakhsh, F. Babaknezhad, Synthesis and characterization of Ni nanoparticles-polyvinylamine/SBA-15 catalyst for simple reduction of aromatic nitro compounds, Catal Commun, 12 (2011) 955-960.
[34] O. Beswick, D. Lamey, F. Muriset, T. LaGrange, L. Oberson, S. Yoon, E. Sulman, P.J. Dyson, L. Kiwi-Minsker, Ni-based structured catalyst for selective 3-phase hydrogenation of nitroaromatics, Catal Today, 273 (2016) 244-251.
[35] J.L. Figueiredo, M.F.R. Pereira, M.M.A. Freitas, J.J.M. Orfao, Modification of the surface chemistry of activated carbons, Carbon, 37 (1999) 1379-1389.
[36] Y. Borodko, S.E. Habas, M. Koebel, P.D. Yang, H. Frei, G.A. Somorjai, Probing the interaction of poly(vinylpyrrolidone) with platinum nanocrystals by UV-Raman and FTIR, J Phys Chem B, 110 (2006) 23052-23059.
[37] M. Crespo-Quesada, J.M. Andanson, A. Yarulin, B. Lim, Y.N. Xia, L. Kiwi-Minsker, UV-Ozone Cleaning of Supported Poly(vinylpyrrolidone)-Stabilized Palladium Nanocubes: Effect of Stabilizer Removal on Morphology and Catalytic Behavior, Langmuir, 27 (2011) 7909-7916.
[38] J. Kimling, M. Maier, B. Okenve, V. Kotaidis, H. Ballot, A. Plech, Turkevich method for gold nanoparticle synthesis revisited, The journal of physical chemistry. B, 110 (2006) 15700-15707.
[39] Y. Xia, Y. Xiong, B. Lim, S.E. Skrabalak, Shape-controlled synthesis of metal nanocrystals: simple chemistry meets complex physics?, Angew Chem, 48 (2009) 60-103.
[40] M. Che, C.O. Bennett, The Influence of Particle-Size on the Catalytic Properties of Supported Metals, Adv Catal, 36 (1989) 55-172.
[41] M. Ruta, N. Semagina, L. Kiwi-Minsker, Monodispersed Pd Nanoparticles for Acetylene Selective Hydrogenation: Particle Size and Support Effects, The Journal of Physical Chemistry C, 112 (2008) 13635-13641.
[42] R. Van Hardeveld, F. Hartog, Surf. Sci., 15 (1969) 189-230.
[43] S. Hub, L. Hilaire, R. Touroude, Hydrogenation of but-1-yne and but-1-ene on Palladium Catalysts - Particle-Size Effect, Applied Catalysis, 36 (1988) 307-322.
[44] A. Quintanilla, V.C.L. Butselaar-Orthlieb, C. Kwakernaak, W.G. Sloof, M.T. Kreutzer, F. Kapteijn, Weakly bound capping agents on gold nanoparticles in catalysis: Surface poison?, Journal of Catalysis, 271 (2010) 104-114.
[45] D.S. Kilin, O.V. Prezhdo, Y.N. Xia, Shape-controlled synthesis of silver nanoparticles: Ab initio study of preferential surface coordination with citric acid, Chem Phys Lett, 458 (2008) 113-116.
[46] W.A. Al-Saidi, H.J. Feng, K.A. Fichthorn, Adsorption of Polyvinylpyrrolidone on Ag Surfaces: Insight into a Structure-Directing Agent, Nano Lett, 12 (2012) 997-1001.
[47] Y. Lu, Y. Mei, M. Ballauff, M. Drechsler, Thermosensitive Core−Shell Particles as Carrier Systems for Metallic Nanoparticles, The Journal of Physical Chemistry B, 110 (2006) 3930-3937.

[48] J.A. Johnson, J.J. Makis, K.A. Marvin, S.E. Rodenbusch, K.J. Stevenson, Size-Dependent Hydrogenation of p-Nitrophenol with Pd Nanoparticles Synthesized with Poly(amido)amine Dendrimer Templates, J. Phys. Chem. C, 117 (2013) 22644-22651.
[49] T.B. Massalski, J.L. Murray, L.H. Bennett, H. Baker, Binary alloy phase diagrams, American Society for Metals, Metals Park, Ohio, 1986.
[50] D.O. Boerma, G. Dorenbos, G.H. Wheatley, T.M. Buck, Atomic Positions of Au Atoms on a Ni(110) Surface, Surface Science, 307 (1994) 674-679.
[51] B.J. Auten, B.P. Hahn, G. Vijayaraghavan, K.J. Stevenson, B.D. Chandler, Preparation and characterization of 3 nm magnetic NiAu nanoparticles, J Phys Chem C, 112 (2008) 5365-5372.
[52] J.L. Figueiredo, Reactivity of coke deposited on metal surfaces, Mater Corros, 50 (1999) 696-699.
[53] J.M.L. Figueiredo, A.R. Boyd, C.R. Stanley, C.N. Ironside, S.G. McMeekin, A.M.P. Leite, Optical modulation at around 1550 nm in an InGaAlAs optical waveguide containing an InGaAs/AlAs resonant tunneling diode, Appl Phys Lett, 75 (1999) 3443-3445.
[54] M.B. Gawande, H.Z. Guo, A.K. Rathi, P.S. Branco, Y.Z. Chen, R.S. Varma, D.L. Peng, First application of core-shell Ag@Ni magnetic nanocatalyst for transfer hydrogenation reactions of aromatic nitro and carbonyl compounds, Rsc Adv, 3 (2013) 1050-1054.
[55] V. Holler, K. Radevik, I. Yuranov, L. Kiwi-Minsker and A. Renken, Reduction of nitrite-ions in water over Pd-supported on structured fibrous materials, App Cat B-Envier, **32** (2001) 143-150.

Tables and figures

Tables

Table 1: Conditions used in the preparation of the Ni NPs.

NPs	*d* (nm)	$NiSO_4 \cdot 6H_2O$	Solvent	PVP (M_W, mass)	Main reducing agent
Ni2	2	0.053 g	Ethylene glycol, 100 cm^3	10’000, 0.22 g	Ethylene glycol
Ni4	4	0.26 g	Ethylene glycol, 50 cm^3	29’000, 2.2 g	$NaBH_4$, 0.1 g
Ni11	11	0.26 g	Ethylene glycol, 120 cm^3	29’000, 2.2 g	$N_2H_4 \cdot H_2O$, 0.1 g
Ni14	14	0.26 g	Tetra-ethyleneglycol, 120 cm^3	29’000, 2.2 g	Tetra-ethyleneglycol

Table 2: Estimated surface atom types for the Ni NPs.

NPs	**Dispersion (%)**	**Fraction (-)**	
		Planes – $x_{\sigma 1}$	**Edges and vertices –$x_{\sigma 2}$**

Ni2	47.6	0.08	0.53
Ni4	25.3	0.34	0.39
Ni11	9.7	0.71	0.17
Ni14	7.7	0.77	0.14

Table 3: The adsorption and kinetic constants obtained from kinetic modelling.

Catalyst	Adsorption constants			Kinetic constants			
	$K_{D,\sigma1}$	$K_{D,\sigma2}$	$K_{N,\sigma1}$	k_1	k_2	k_3	k_4
	($l\ mol^{-1}$)			($mmol_{m\text{-DNB}}\ mol_{Ni}^{-1}\ min^{-1}$)			
Ni2	330 ± 30	4.0	43 ± 1	0.21	0.86	0.04	-
Ni14				0.15	0.40	0.05	0.03
$Ni2/ACF_{UVO}$	550 ± 50	5.9 ± 1	73 ± 3	0.37	0.12	0.75	-
$Ni14/ACF_{UVO}$				0.26	0.20	0.28	0.02

Figures captions

Figure 1: (A) Representative HRTEM image and **(B)** associated particle size distribution of the Ni4 NPs.

Figure 2: (A) TOF (open bars) and fraction of planes $x_{\sigma2}$ (square symbols) and **(B)** Selectivity to *m*-NAN for unsupported Ni NPs at 50% (hatched bars) and 99% conversion (solid bars). *Reaction conditions:* $C_{m\text{-DNB},0} = 3.7 \cdot 10^{-3}$ mol·l^{-1}, 80 cm^3 of MeOH, P_{H2} = 6.1 bar, P_{tot} = 20 bar, T = 423 K, *m*-DNB:Ni = 58.

Figure 3: Variation of TOF (open bars) and selectivity to *m*-NAN (solid bars) over monodispersed (2 and 14 nm) Ni NPs/ACF treated by UV-Ozone or pyrolysis. *Reaction conditions*: $C_{m\text{-DNB},0} = 3.7 \cdot 10^{-3}$ mol·l^{-1}, 80 cm^3 of MeOH, P_{H2} = 6.1 bar, P_{tot} = 20 bar, T = 423 K, *m*-DNB:Ni for the $Ni2/ACF_{UVO}$, $Ni2/ACF_{\Delta T}$, $Ni14/ACF_{UVO}$, $Ni14/ACF_{\Delta T}$ = 31, 55, 32 and 62, respectively. Nickel loading (wt.%) = 1.79, 1.99, 2.56, 1.25, respectively (same order than for the *m*-DNB:Ni ratio).

Figure 4: (A) Evolution of the molar fraction of (●) *m*-DNB, (■) *m*-NAN and (▲) *m*-PDA with time over cleaned supported 2 nm Ni NPs cleaned by UVO, $Ni2/ACF_{UVO}$; variation of

selectivity with conversion for unsupported Ni (open symbols) and Ni/ACF_{UVO} catalysts (full symbols) for (**B**) Ni2 and (**C**) Ni14 NPs. Reaction conditions: $C_{m\text{-DNB},0} = 3.7 \cdot 10^{-3}$ mol·l^{-1}, 80 cm^3 of MeOH, $P_{H2} = 6.1$ bar, $P_{tot} = 20$ bar, $T = 423$ K, *m*-DNB:Ni = 58, 31, 58 and 32 for Ni2, Ni2/ACF_{UVO}, Ni14 and Ni14/ACF_{UVO}, respectively. Nickel loading (wt.%): (Ni2/ACF_{UVO}, Ni14/ACF_{UVO}) = 1.79, 2.56, respectively.

Figure 5: Reaction pathways associated with the hydrogenation of *m*-DNB to *m*-NAN and *m*-PDA. The targeted partial hydrogenation and undesired routes leading to hydrogenation of both nitro group are represented by bold and dashed arrows, respectively.

Figure 6: Experimental (●) *m*-DNB, (■) *m*-NAN and (▲) *m*-PDA and modelled (lines) concentration *vs.* time for (**A**) Ni2, (**B**) Ni2/ACF_{UVO}, (**C**), Ni14 (**D**) Ni14/ACF_{UVO}. Reaction conditions: $C_{m\text{-DNB},0} = 3.7 \cdot 10^{-3}$ mol·l^{-1}, 80 cm^3 of MeOH, $P_{H2} = 6.1$ bar, $P_{tot} = 20$ bar, $T = 423$ K, *m*-DNB:Ni = 58, 31, 58 and 32 for Ni2, Ni2/ACF_{UVO}, Ni14 and Ni14/ACF_{UVO}, respectively. Ni loading (wt.%): (Ni2/ACF_{UVO}, Ni14/ACF_{UVO}) = 1.79, 2.56, respectively.

Figure 7: Representative HRTEM images of (**A**) Au7 and (**C**) Ni-Au PVP-stabilized NPs and associated metal particle size distributions (**B** and **D**).

Figure 8: EDX Spectrum of the Ni-Au NPs.

Figure 9: XRD profiles of Ni4, Au7 and Ni-Au colloids.

Figure 10: Variation of turnover frequency (TOF) (open bars) and selectivity to *m*-NAN (solid bars) using dispersed Ni2, Au7 and Ni-Au NPs and supported Ni2/ACF_{UVO} and Ni-Au/ACF_{UVO} catalysts. $C_{m\text{-DNB},0} = 3.7 \cdot 10^{-3}$ mol·l^{-1}, 80 cm^3 of MeOH, $P_{H2} = 6.1$ bar, $P_{tot} = 20$ bar, $T = 423$ K, *m*-DNB:Me = 58, 58, 58, 31 and 58 for Ni2, Au7, Ni-Au, Ni2/ACF_{UVO} and Ni-Au/ACF_{UVO}. Ni loading (wt.%): (Ni2/ACF_{UVO}, Ni-Au/ACF_{UVO}) = 1.79, 1.28, respectively.

*Graphical Abstract

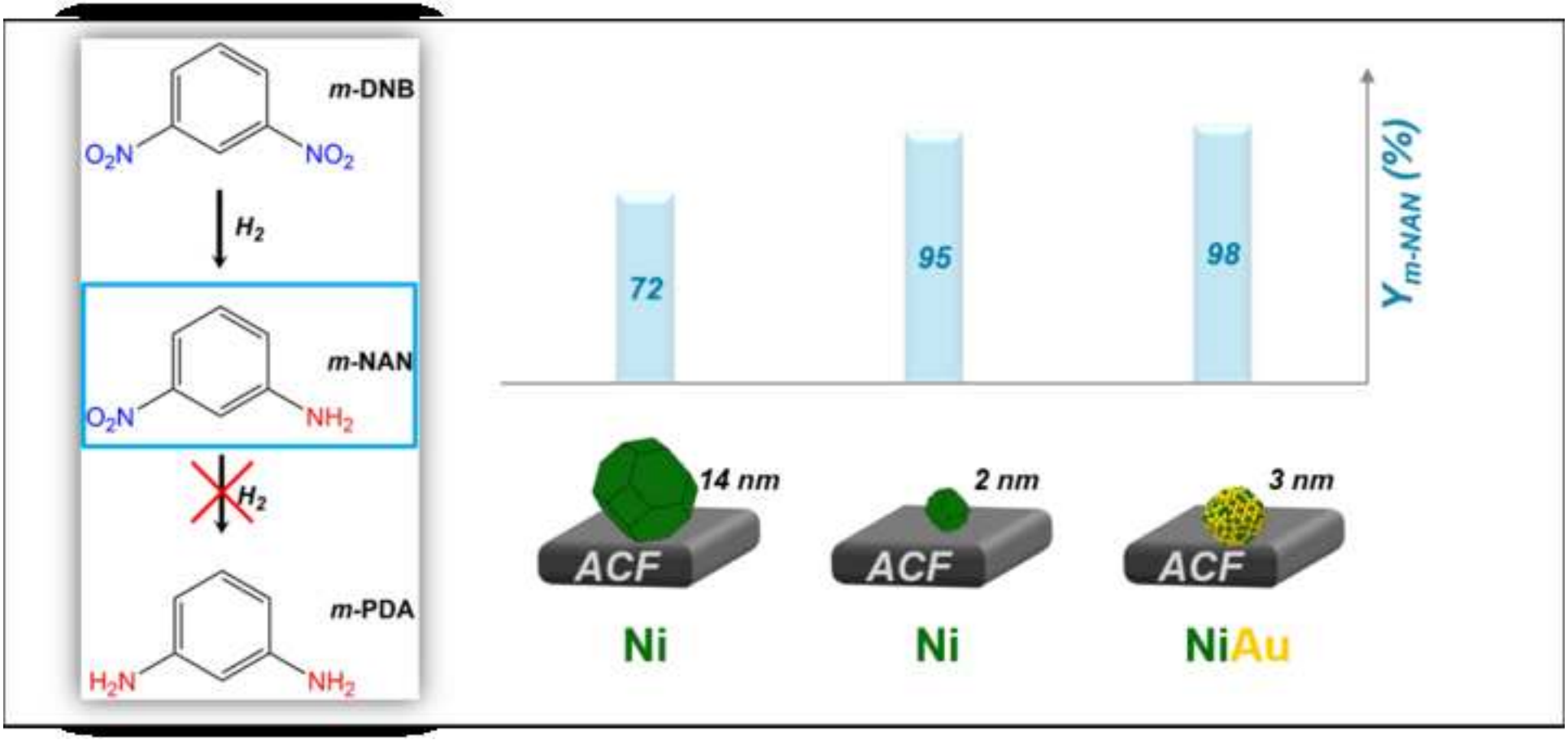

1 Highlights

- The partial hydrogenation of *meta*-dinitrobenzene (*m*-DNB) to *meta*-nitroaniline (*m*-NAN) showed to be structure-sensitive over PVP-stabilized Ni° nanoparticles (NPs) of 2–14 nm
- The yield to *m*-NAN ($Y_{m\text{-}NAN}$ =96%) was optimized by supporting the 2 nm Ni NPs on activated carbon fibres (ACF) as structured support while the highest *turnover frequency* was afforded by the largest crystallites
- The catalytic data were rationalized using the Langmuir-Hinshelwood kinetic model assuming a two-sites mechanism (the edge/vertex and plane atoms)
- The selectivity ($S_{m\text{-}NAN}$ =99%) and activity towards *m*-NAN were further enhanced over bimetallic Ni-Au NPs supported on ACF

Figure 6 revised

Click here to download high resolution image

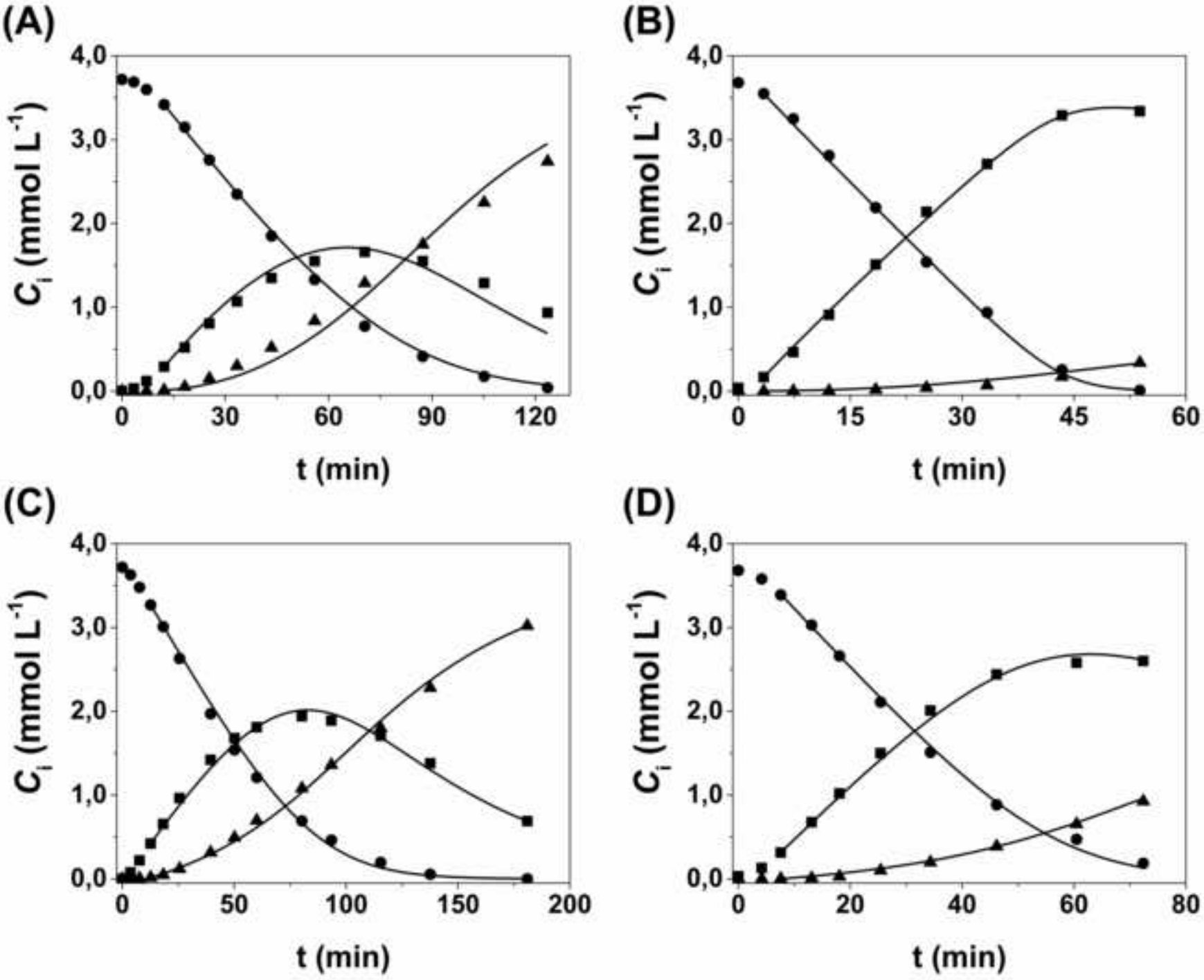

Figure 1

Click here to download high resolution image

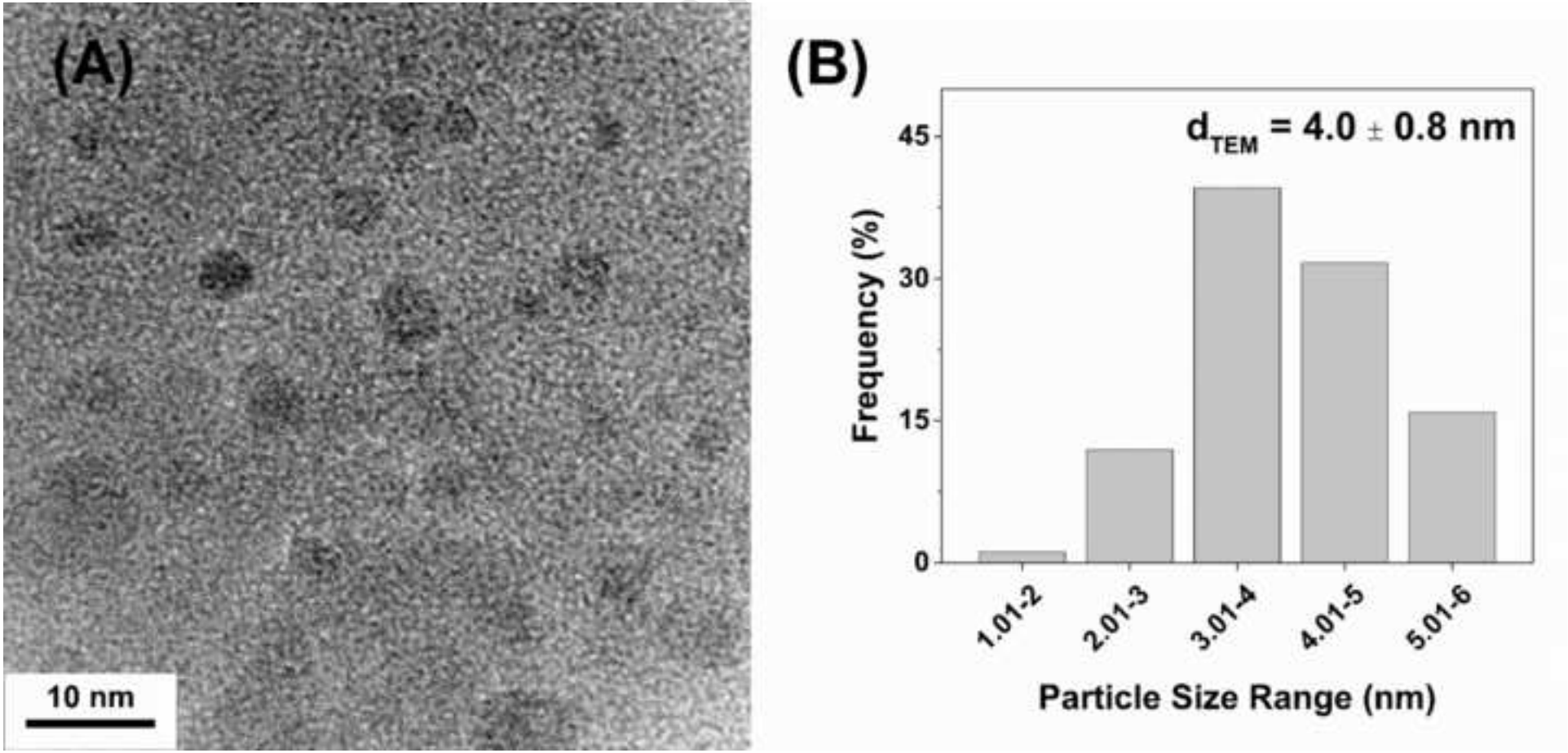

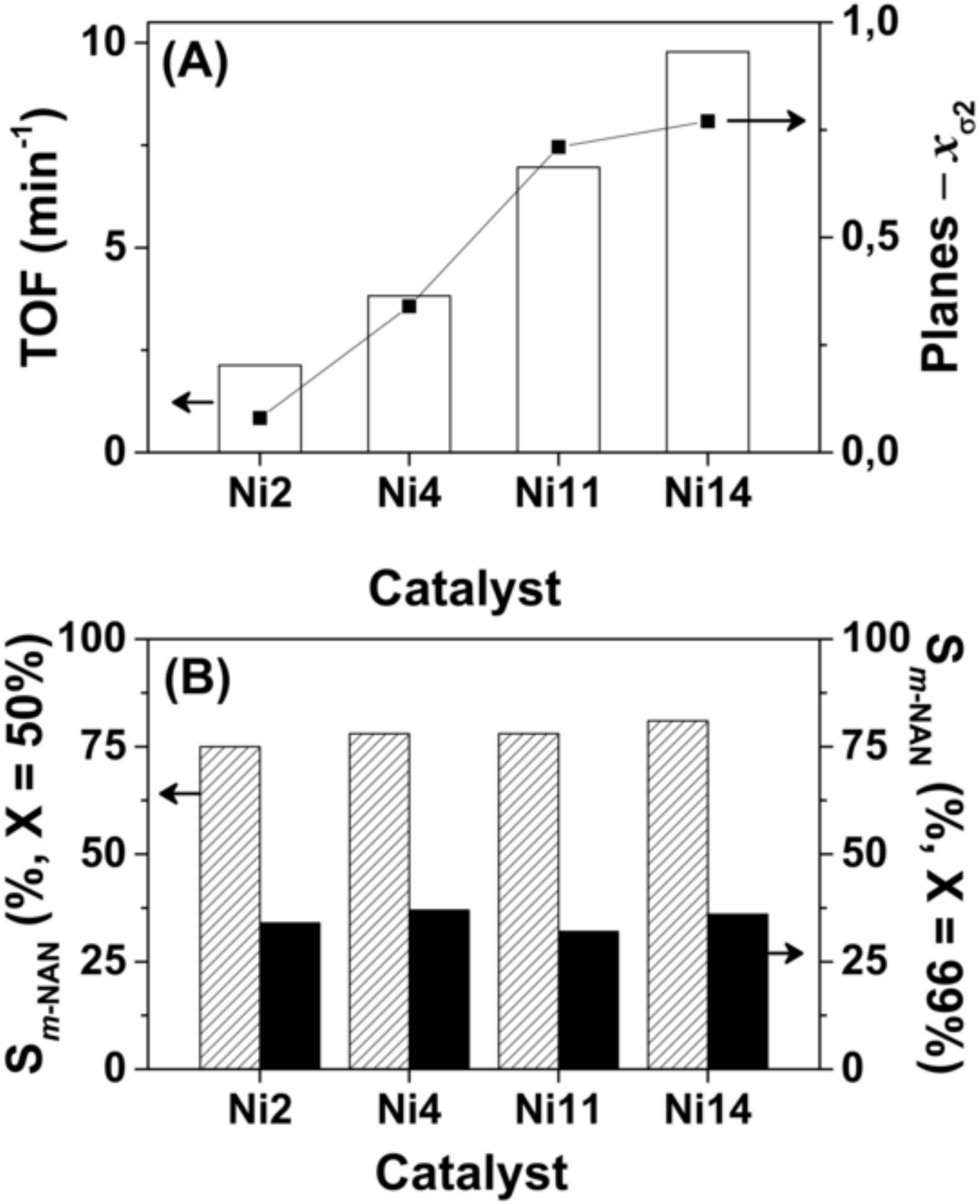
(A)
TOF (min-1)
Planes – xσ2
10
5
0
1,0
0,5
0,0
Ni2
Ni4
Ni11
Ni14
Catalyst
(B)
Sm-NAN (%, X = 50%)
Sm-NAN (%, X = 99%)
100
75
50
25
0
Ni2
Ni4
Ni11
Ni14
Catalyst

Figure 3

Click here to download high resolution image

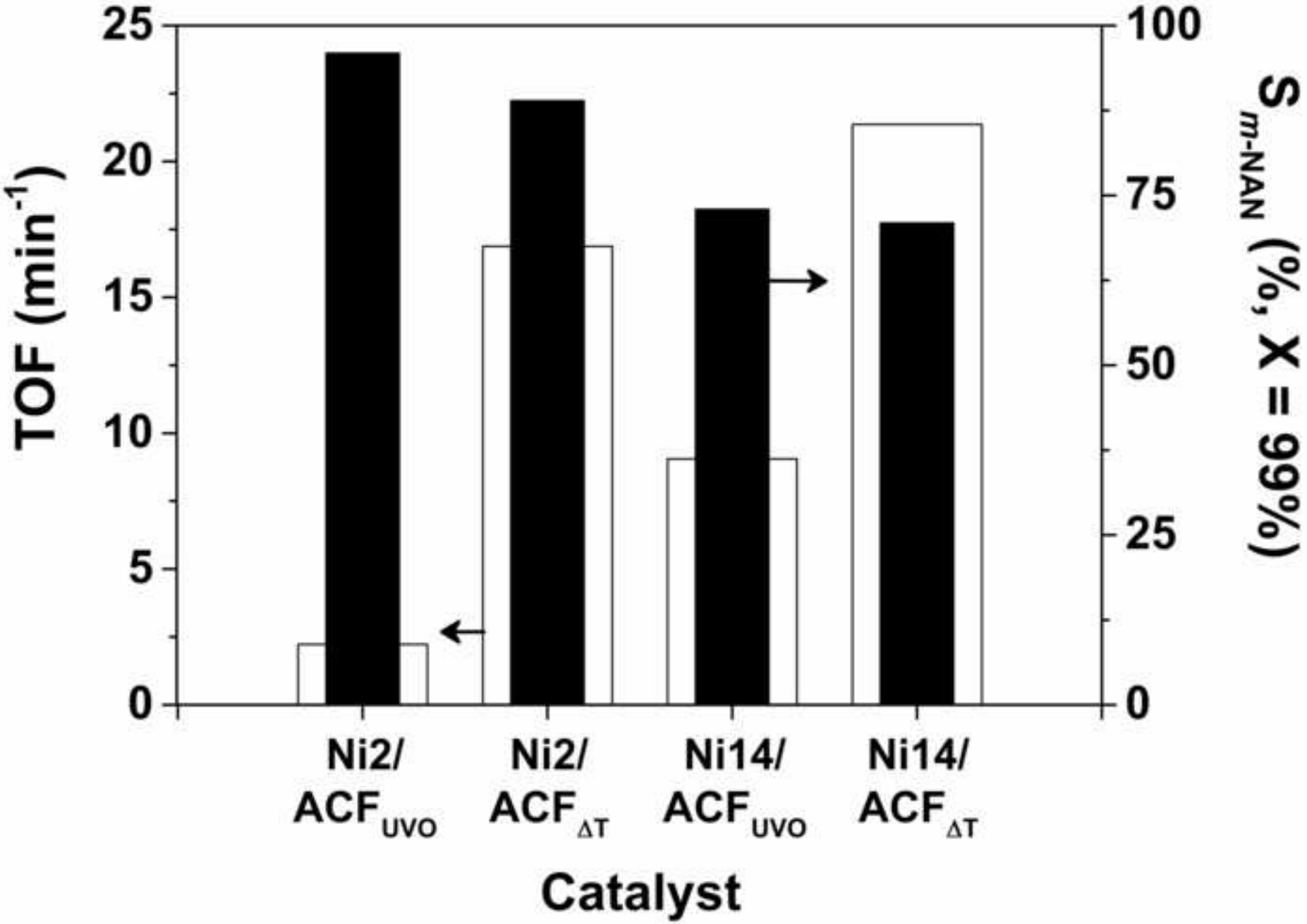

Figure 4

Click here to download high resolution image

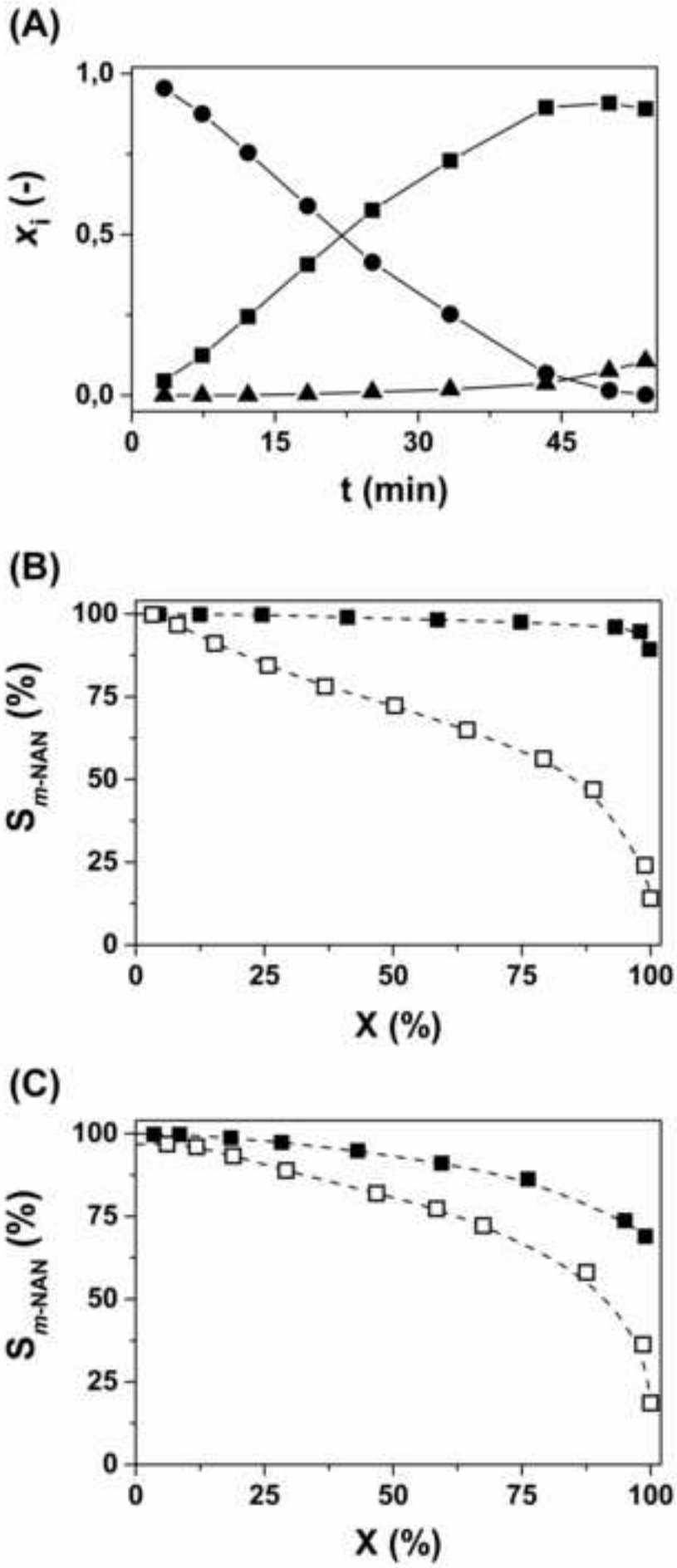

Figure 5

Click here to download high resolution image

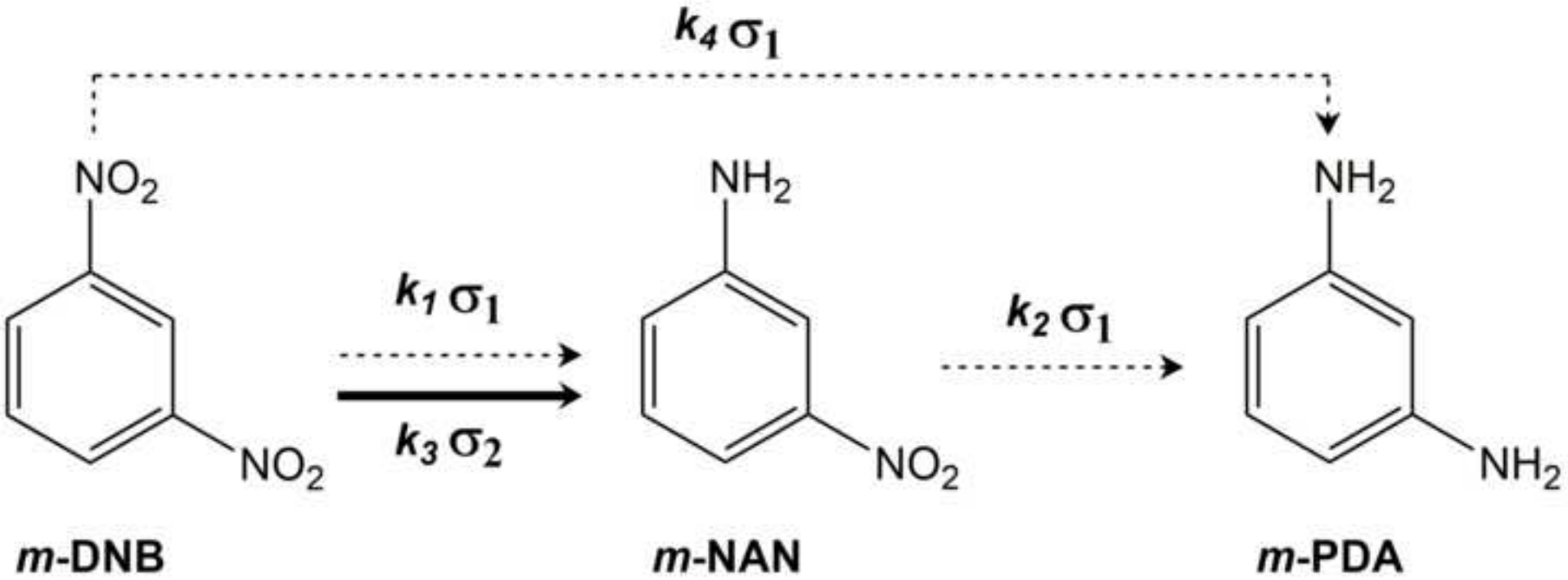

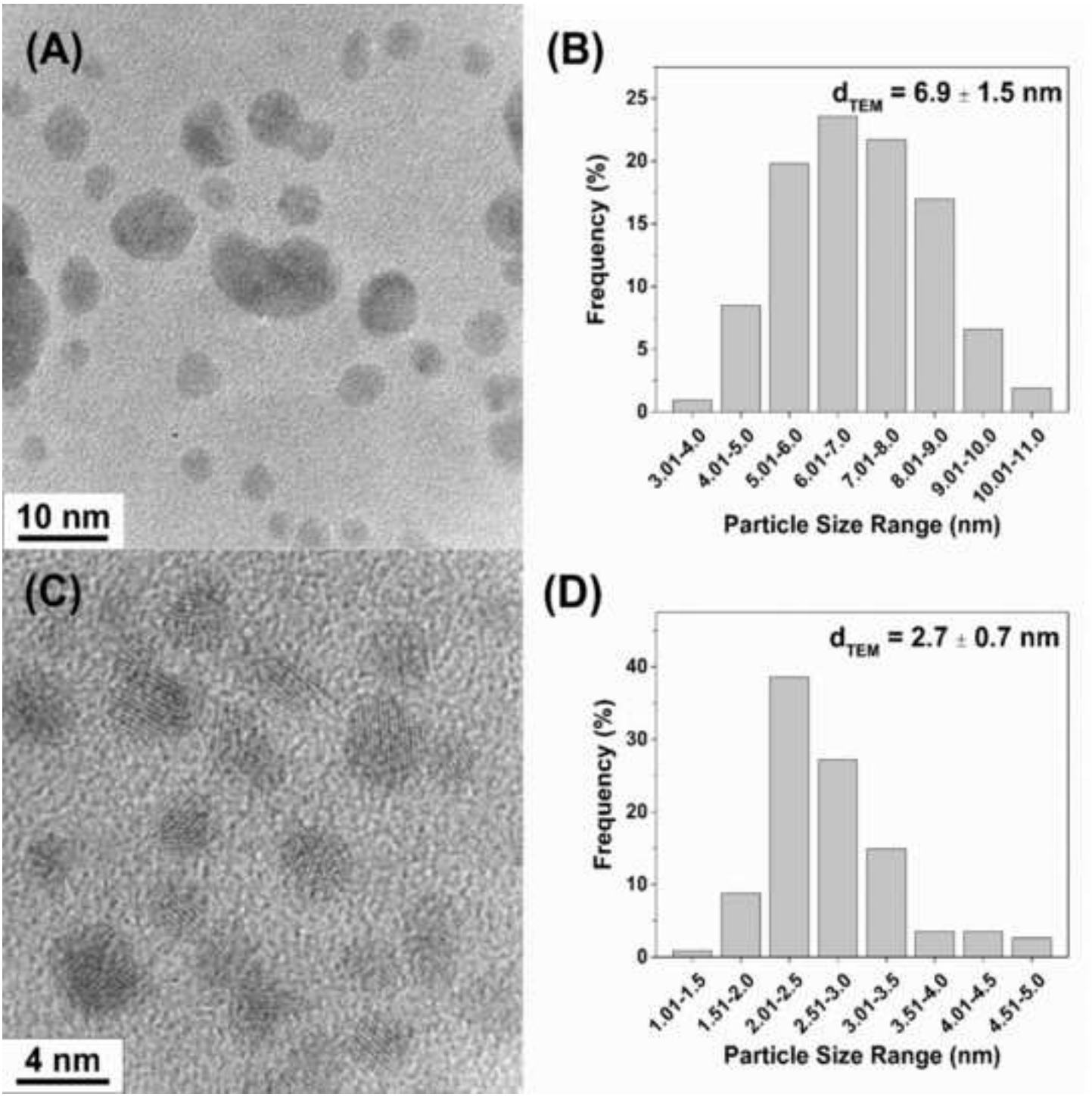
(A)
10 nm
(B)
d_{TEM} = 6.9 ± 1.5 nm
Frequency (%)
0
5
10
15
20
25
3.01-4.0
4.01-5.0
5.01-6.0
6.01-7.0
7.01-8.0
8.01-9.0
9.01-10.0
10.01-11.0
Particle Size Range (nm)
(C)
4 nm
(D)
d_{TEM} = 2.7 ± 0.7 nm
Frequency (%)
0
10
20
30
40
1.01-1.5
1.51-2.0
2.01-2.5
2.51-3.0
3.01-3.5
3.51-4.0
4.01-4.5
4.51-5.0
Particle Size Range (nm)

Figure 8

Click here to download high resolution image

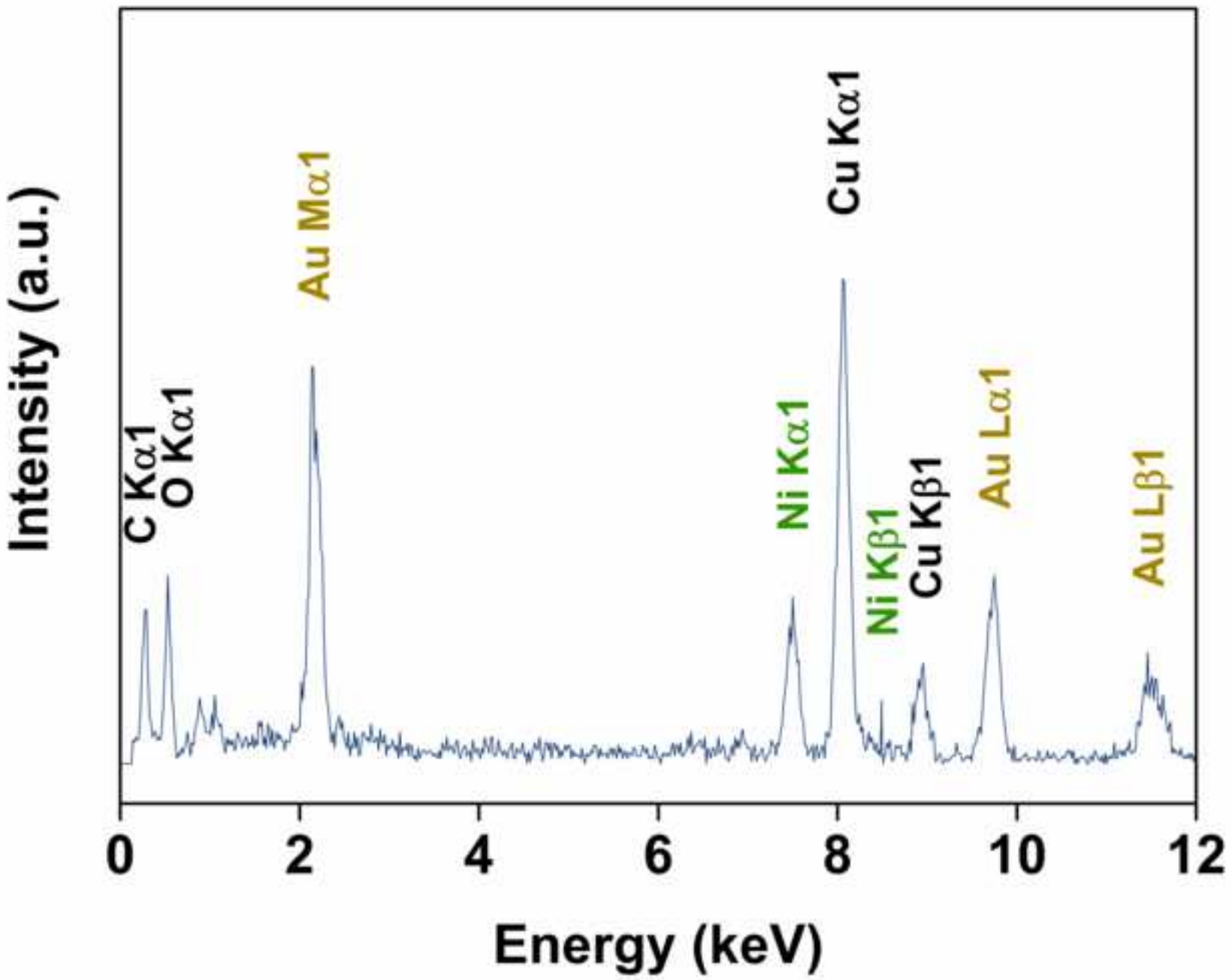

Figure 9
Click here to download high resolution image

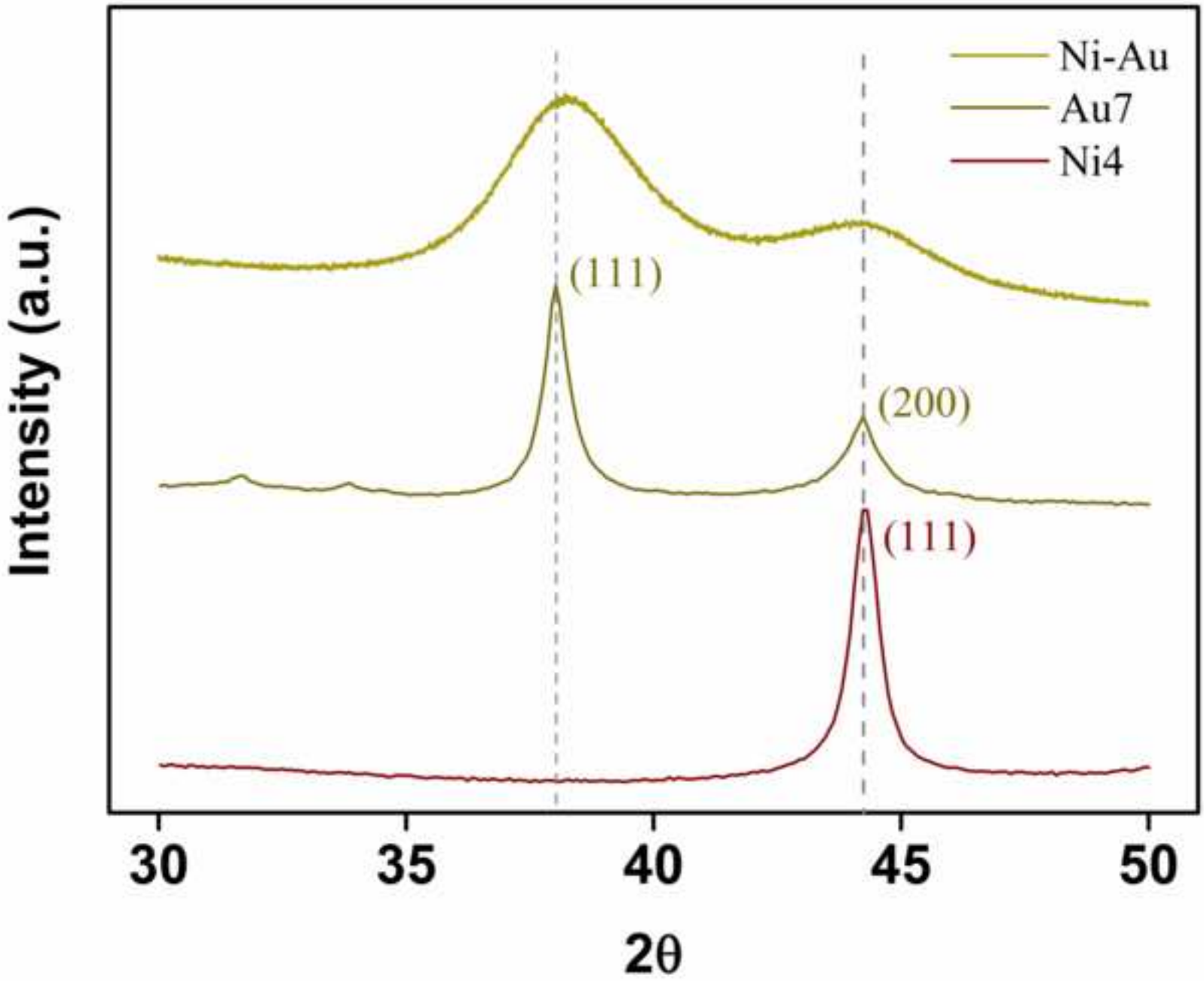

Figure 10

Click here to download high resolution image

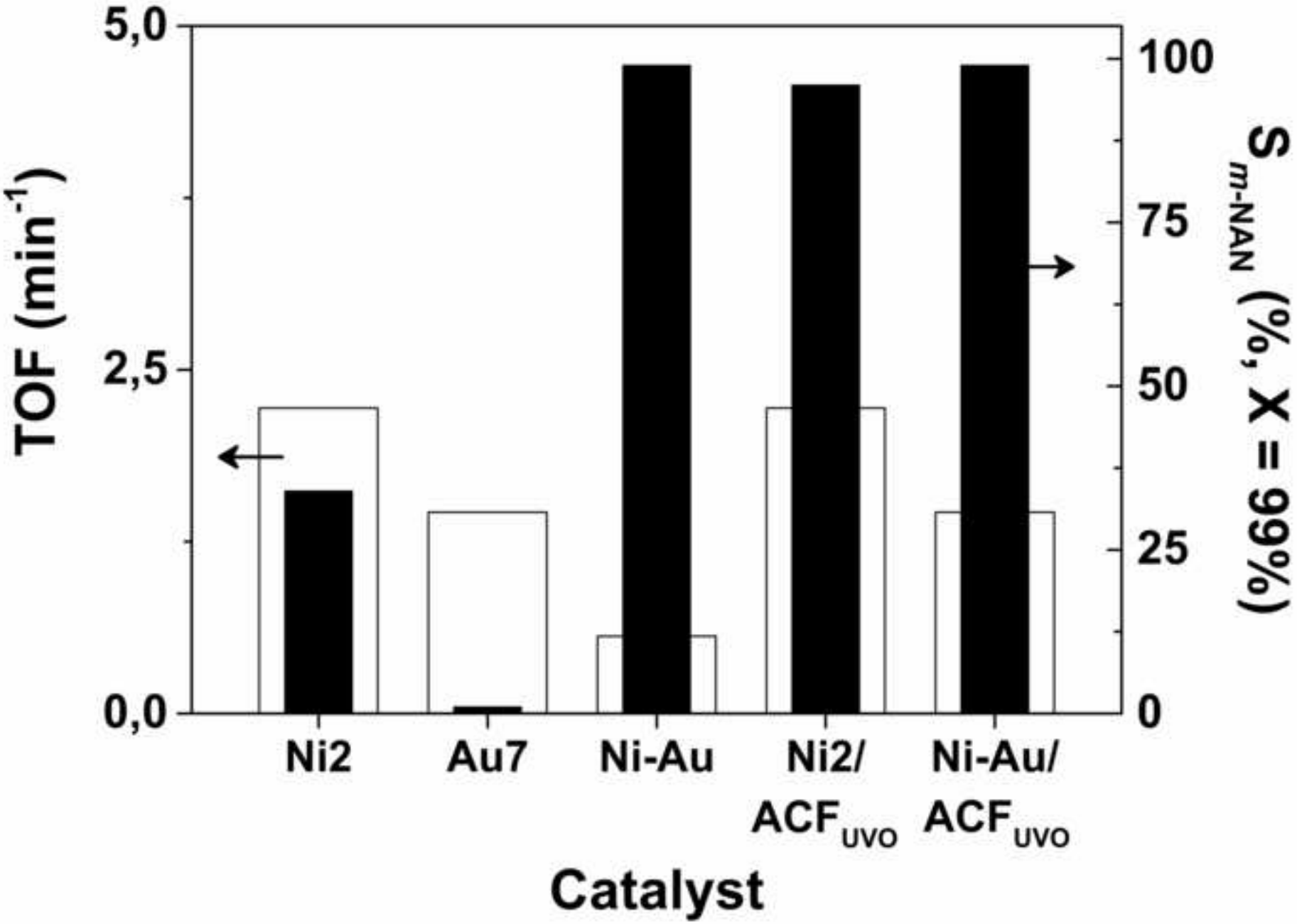

5 Highlights

- The partial hydrogenation of *meta*-dinitrobenzene (*m*-DNB) to *meta*-nitroaniline (*m*-NAN) showed to be structure-sensitive over PVP-stabilized Ni° nanoparticles (NPs) of 2□14 nm
- The yield to *m*-NAN ($Y_{m\text{-}NAN}$ =96%) was optimized by supporting the 2 nm Ni NPs on activated carbon fibres (ACF) as structured support while the highest *turnover frequency* was afforded by the largest crystallites
- The catalytic data were rationalized using the Langmuir-Hinshelwood kinetic model assuming a two-sites mechanism (the edge/vertex and plane atoms)
- The selectivity ($S_{m\text{-}NAN}$ =99%) and activity towards *m*-NAN were further enhanced over bimetallic Ni-Au NPs supported on ACF